ON THE MECHANICAL BEHAVIOUR OF A BUTT JOINTED THERMOPLASTIC COMPOSITE UNDER BENDING

Ismet Baran[1], Laurent Warnet[2] and Remko Akkerman[3]

[1]Faculty of Engineering Technology, University of Twente
P.O. Box 217, 7500AE, Enschede, The Netherlands
Email: i.baran@utwente.nl, web page: http://www.utwente.nl

[2]Faculty of Engineering Technology, University of Twente
P.O. Box 217, 7500AE, Enschede, The Netherlands
Email: l.warnet@utwente.nl, web page: http://www.utwente.nl

[3]Faculty of Engineering Technology, University of Twente
P.O. Box 217, 7500AE, Enschede, The Netherlands
Email: r.akkerman@utwente.nl, web page: http://www.utwente.nl

Keywords: Butt-joint, FEM, Cohesive surface, VCCT, Thermoplastic composite

ABSTRACT

In the present work, the mechanical behavior of a recently developed novel butt jointed thermoplastic composite was investigated under bending conditions. The laminated skin and the web were made of carbon fiber (AS4) and polyetherketoneketone (PEKK). The butt joint (filler) was injection molded from 20% short carbon fiber filled with PEKK thermoplastic. The skin and web were co-consolidated together with the butt joint in the form of a hybrid T-shaped structure. A three point bending (3 PB) set-up was used to investigate the mechanical response of the hybrid composite. The crack initiation and propagation mechanisms for the filler and the delamination at the skin-filler interface were captured using a high speed camera. It was found from the experimental observations that the crack initiated in the filler and then propagated towards the skin-filler interface. A numerical model was also developed using the finite element method in ABAQUS including the crack initiation and growth in the filler together with the delamination at the skin-filler interface. For this purpose the virtual crack closure technique (VCCT) was employed for the crack growth in the filler and the traction separation law was applied at the skin-filler interface using a cohesive surface. The residual stresses and deformations coming from the co-consolidation process were predicted by applying a thermal load and taken into account in the quasi-static analysis. A good agreement was found between the predicted and measured force-displacement curves. The developed numerical model was further employed to address the crack initiation and growth in the filler and delamination at the skin-filler interface using the mix mode effective fracture energies. A linear elastic behavior was found in the structure until the crack initiation in the filler.

1 INTRODUCTION

The usage of thermoplastic composites (TPCs) has been gradually increasing in the aircraft and automotive industries owing to their high toughness to weight ratio and versatile processing capabilities. In particular, thermoplastic stiffened composites are currently being developed for primary aircraft components such as fuselage and torsion box at airplane tail. Thermoplastic composites are manufactured using various process techniques: stamp forming, laser assisted tape laying, welding, injection molding, co-consolidation in autoclave, over-molding, etc.

The TPCs have still been under development with novel material compositions and manufacturing techniques. There have been several studies carried out in literature to characterize the material and understand the forming conditions as well as mechanical performance [1-10]. Moreover, the fracture behavior of TPCs has been investigated in [11-13] with a focus on delamination which is one of the predominant failure type in many laminated composite systems.

A recently developed hybrid composite structure made of polyetherketoneketone (PEKK) thermoplastic reinforced with carbon fiber (AS4) was considered in the present work. The continuous reinforced AS4/PEKK laminates (skin and web) were co-consolidated using an injection molded butt joint (filler) made of short fiber reinforced AS4/PEKK. The mechanical response of the hybrid T-shaped structure was investigated under three point bending (3 PB) conditions. The crack initiation and propagation in the filler as well as delamination at the skin-filler interface were captured using a high speed camera. A quasi-static model was developed to predict the force-displacement response and the fracture behavior using the finite element method (FEM) in ABAQUS [14]. The thermal residual stresses were also taken in to account in model.

2 EXPERIMENTS

The mechanical response of the hybrid butt jointed composite was observed under 3 PB test conditions. The laminated skin and web made of AS4/PEKK were produced using an autoclave tooling. Subsequently, 20% short carbon filled PEKK FC (fast cooled) filler material was injected molded as a butt joint. A schematic view of the test set-up and the cross section of the hybrid joint are shown in Fig. 1 (*left*) and Fig. 1 (*right*), respectively. The skin and web had the symmetric ply orientation with 16 layers $[0/45/-45/90/45/0/-45/90]_s$. The fiber direction of the 0° ply was oriented in the *x*-direction for the skin and in the *y*-direction for the web. The aligned short fibers are oriented in the *z*-direction.

The specimens were cut from a relatively large panel into small pieces and prepared with a nominal width of 14.9 mm and a nominal length of 70 mm with a span length of 57 mm. The side surfaces of each specimens were then manually grinded in water. The thickness of the skin was found to be varying throughout the stiffened panel due to the process induced effects such as residual stresses and shape distortions [15-17]. In this work, three specimens taken from different places along the butt jointed panel were presented. The utilized three different skin thicknesses (*h* in Fig. 1 (*left*)) values were 2.71 mm, 2.303 mm and 2.29 mm. The nominal radius of the filler was 6 mm. The quasi-static 3 PB tests were carried out using a 10 kN capacity Zwick uniaxial tensile system. The initiation and growth of the crack as well the post delamination behavior was captured using a high speed camera during the 3 PB tests. For this purpose, the camera focused on the full width of the filler, in the region of its interaction with the skin.

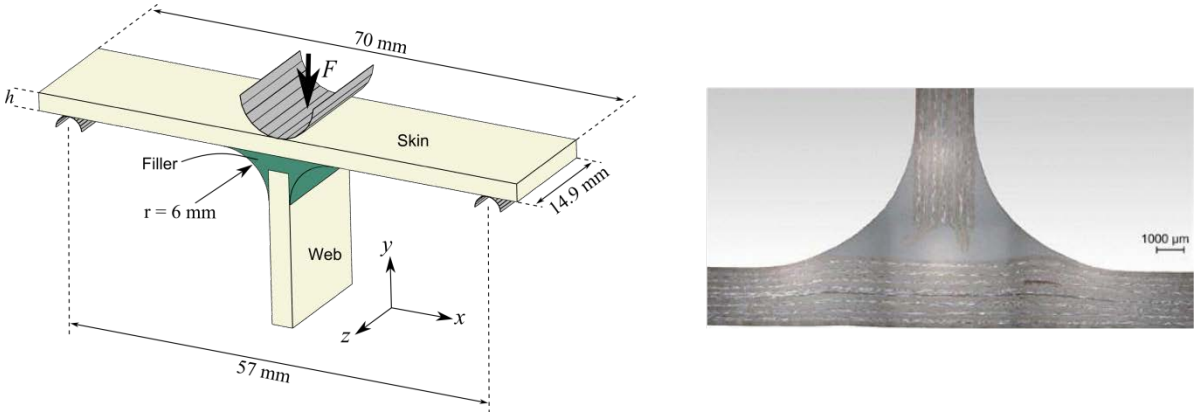

Figure 1: The schematic view of the 3 PB test set-up (*left*). Cross section of the hybrid butt joint (*right*).

3 NUMERICAL MODELLING

The 3 PB test was simulated using a quasi-static analysis in ABAQUS [14]. In order to reflect the actual fiber orientation for the skin and web as well as filler a three dimensional (3D) model was developed. A schematic view of the model with the enmeshment is depicted in Fig. 2. A cohesive surface was defined at the skin-filler interface using a traction separation law to simulate the delamination. Moreover, the virtual crack closure technique (VCCT) was implemented to predict the

crack initiation and growth in the filler. Since the crack initiated only from one curved part of the filler according to the experiments, only half of the filler domain was included in the VCCT as seen in Fig. 2 (*right*). The support and loading pins were modelled using rigid analytic surfaces since the pins had much higher stiffness than the composite and the pin deformations were neglected. A mechanical contact formulation was defined at the pin-skin and support-skin interface which allowed any sliding and restricted any penetration of the skin beyond the rigid surfaces.

Two different loading steps were used in the numerical simulations. In the first step, a thermal load was introduced to the hybrid composite structure by applying a temperature gradient ΔT and the thermal stresses were predicted. In the second step, a displacement (d) was applied at the reference point (RP) seen in Fig. 2 (*left*) in the negative y-direction. The details of the considered values for ΔT and d together with the material properties are provided in Section 3.3.

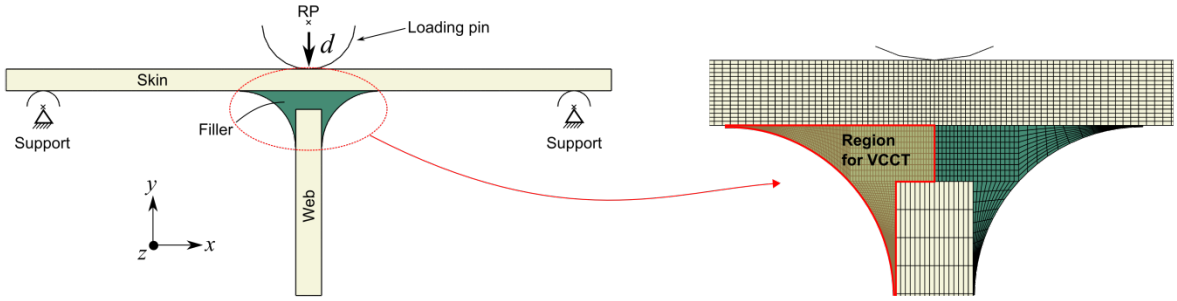

Figure 2: Schematic view of the geometry in numerical model (*left*). The details of the enmeshment and region for VCCT shown with shaded area (*right*).

3.1 Delamination at the skin-filler interface

An uncoupled linear elastic traction separation law was utilized in ABAQUS to simulate the damage initiation and evolution for the cohesive surface. The normal and shear stresses are related with the normal and shear separations across the cohesive interface, i.e. skin-filler interface. The uncoupled elastic behavior can be written as:

$$\mathbf{t} = \begin{Bmatrix} t_n \\ t_s \\ t_t \end{Bmatrix} = \begin{bmatrix} K_{nn} & 0 & 0 \\ 0 & K_{ss} & 0 \\ 0 & 0 & K_{tt} \end{bmatrix} \begin{Bmatrix} \delta_n \\ \delta_s \\ \delta_t \end{Bmatrix} \tag{1}$$

where **t** is the nominal traction stress vector consisting of three components t_n (in the normal direction to the cohesive surface), t_s (in the first shear direction) and t_t (in the second shear direction). The corresponding separations at the interface are denoted by δ_n, δ_s and δ_t. It is seen in Eq. 1 that the contact stiffness components (K_{nn}, K_{ss} and K_{tt}) are not coupled, i.e. pure normal or tangential separations will not contribute to the cohesive forces in the other directions. The damage initiation, which is the beginning of the degradation of the cohesive surface, is defined based on the linear elastic relation in Eq. 1. The process of degradation begins when the contact stresses and/or contact separations satisfy certain damage initiation criteria. For this, a quadratic stress criterion was considered as described in Eq. 2.

$$\left(\frac{t_n}{t_n^o}\right)^2 + \left(\frac{t_s}{t_s^o}\right)^2 + \left(\frac{t_t}{t_t^o}\right)^2 = 1 \tag{2}$$

where t_n^o, t_s^o and t_t^o are the peak values of the contact stress. It should be noted that t_n must be positive (in tension) in order to initiate the delamination at the interface.

A linear degradation is used for the damage evolution. A scalar damage variable *D* is defined representing the overall damage at the contact. Initially *D* is equal to 0 and monotonically increases to 1 during the progression of the damage. Hence, the contact stress is affected by the damage variable according to the following relation:

$$\mathbf{t} = (1-\mathrm{D})\bar{\mathbf{t}} \tag{3}$$

where $\bar{\mathbf{t}}$ is the contact stress vector predicted using the relation in Eq. 1 with the current separations without damage. A mix mode cohesive behavior was implemented for the damage evolution based on the fracture energies of Mode-1 (tensile opening), Mode-II (in-plane opening) and Mode-III (out-of-plane opening). The fracture energies during the separation of the cohesive surface are defined as:

$$G_I = \frac{t_n^o \delta_n^f}{2}, G_{II} = \frac{t_s^o \delta_s^f}{2}, G_{III} = \frac{t_t^o \delta_t^f}{2} \tag{4}$$

where G_I, G_{II} and G_{III} are the fracture energies of Mode-1, Mode-II and Mode-III, respectively. δ_n^f, δ_s^f and δ_t^f are the complete (or final) separations in the normal (Mode-I), first shear (Mode-II) and second shear (Mode-III) directions, respectively. The Benzeggagh-Kenane (BK) fracture criterion [14, 18] was used to define the mix mode softening of the cohesive surface. The corresponding expression is written as:

$$G_{mc} = G_{Ic} + (G_{IIc} - G_{IIIc})\left(\frac{G_{II} + G_{III}}{G_I + G_{II} + G_{III}}\right)^{\eta} \tag{5}$$

where G_{mc} is the critical fracture energy of the mix mode behavior, G_{Ic}, G_{IIc} and G_{IIIc} are the critical fracture energies of Mode-I, Mode-II and Mode-III, respectively, and η is the cohesive property parameter. A schematic representation of the mix mode damage evolution is depicted in Fig. 3(*left*). The complete damage takes place when the fracture energy of the mix mode (G_m) is equal or larger than G_{mc}. This relation can be written as:

$$G_m = \frac{t_m^o \delta_m^f}{2} \geq G_{mc} \tag{6}$$

where t_m^o is the peak value of the contact stress calculated using the mix mode law and δ_m^f is the corresponding effective complete separation. The linear damage variable *D* used in Eq. 3 can then be calculated as:

$$D = \frac{\delta_m^f (\delta_m^{\max} - \delta_m^o)}{\delta_m^{\max} (\delta_m^f - \delta_m^o)} \tag{7}$$

where δ_m^o is the effective separation at damage initiation, $\delta_m^{\max}$ is the maximum separation obtained at the cohesive surface. The linear degradation of the stiffness is shown in Fig. 3 (*right*). If there is an unloading subsequent to damage initiation, it occurs linearly towards the origin of the traction-separation plane as shown in Fig. 3 (*right*). Reloading subsequent to unloading also occurs along the same linear path until the softening envelope (line AB) is reached.

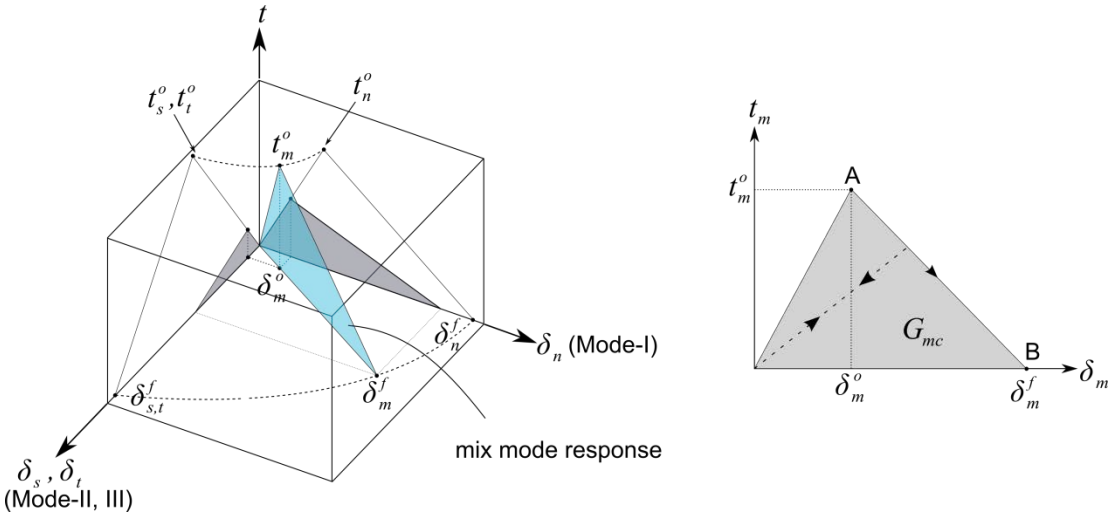

Figure 3: Mix mode damage evolution (*left*). Linear softening law (*right*).

3.2 Crack initiation and propagation in the filler

The VCCT uses the principles of linear elastic fracture mechanics (LEFM) and hence is convenient for applications in which brittle crack propagation takes place. This choice was partly supported by the fact that the filler failed in a brittle way in the butt joint structure during the 3 PB tests, without significant sign of plastic behavior (see Section 4). The crack initiation was defined using the maximum principal stress criterion for the filler material. Once the principle stress value of an element is equal or higher than the critical principal stress (S_c), than a damage is initiated in that particular element [14].

The VCCT is based on the assumption that the strain energy released, when a crack is extended by a certain amount, is the same as the energy required to close the crack by the same amount [19, 20]. For instance, the energy released when the crack is extended by Δx from x to $x+\Delta x$ as seen in Fig. 4 is identical to the energy required to close the crack between location i and i^* (closure of element E1 and element E2 in Fig. 4). Fig. 4 shows a 3D crack model in which the z-direction is in the out-of-plane direction and the model has a thickness of Δz in the z-direction. The total work required to close the crack along one element, i.e. the crack between element E1 and element E2, can be written as:

$$\Delta E = \frac{1}{2}\left[F_{y,j}\left(v_i - v_{i^*}\right) + F_{\mathrm{x},j}\left(u_i - u_{i^*}\right) + F_{\mathrm{z},j}\left(w_i - w_{i^*}\right)\right] \tag{8}$$

where $F_{x,j}$, $F_{\mathrm{y},j}$ and $F_{\mathrm{z},j}$ are the forces acting on node j in the x-, y- and z-direction, respectively, u_i, v_i and w_i are the displacements at node i and similarly u_{i^*}, v_{i^*} and w_{i^*} are the displacements at node i^* in the x-, y- and z-direction, respectively. The strain energy release rate G can be defined as the ratio between the total work (ΔE) and the crack surface ($\Delta x \Delta z$). The components of the strain energy release rate (G_I, G_{II} and G_{III}) for Mode-I, Mode-II and Mode-III can be calculated as [14, 21]:

$$\begin{aligned} G_I &= \frac{1}{2\Delta x \Delta z}\left[F_{y,j}\left(v_i - v_{i^*}\right)\right] \\ G_{II} &= \frac{1}{2\Delta x \Delta z}\left[F_{\mathrm{x},j}\left(u_i - u_{i^*}\right)\right] \\ G_{III} &= \frac{1}{2\Delta x \Delta z}\left[F_{\mathrm{z},j}\left(w_i - w_{i^*}\right)\right] \end{aligned} \tag{9}$$

The crack tip is debonded when the effective strain energy release rate at the crack surface is equal

or larger than the effective critical strain energy release rate (G_m^c) which is defined using the BK law:

$$G_m^c = G_I^c + (G_{II}^c - G_{III}^c)\left(\frac{G_{II}+G_{III}}{G_I+G_{II}+G_{III}}\right)^{\eta} \tag{10}$$

where G_I^c, G_{II}^c and G_{III}^c are the critical energy release rate of Mode-1, Mode-II and Mode-III, respectively.

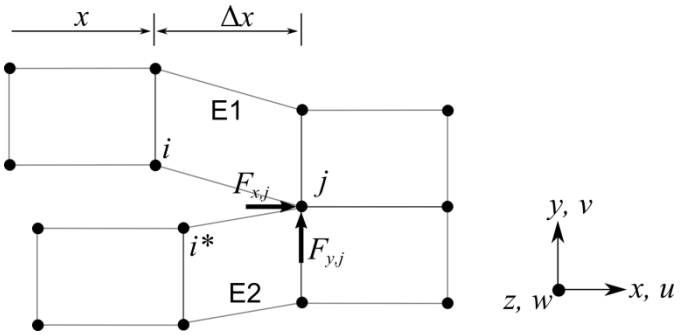

Figure 4: Representation of the Virtual Crack Closure Technique (VCCT).

3.3 Model parameters

The linear elastic properties of the filler were measured for an injection molded dog-bone specimens. For this purpose Zwick Z100 tensile machine was used to obtain the mechanical properties in the longitudinal and transverse directions. The coefficient of thermal expansion of the filler material in the longitudinal (α_1) and transverse ($\alpha_2 = \alpha_2$) direction was measured using a thermo-mechanical analyzer. The obtained values for the filler material properties are given in Table 1. The transverse strength of the filler was also measured using a separate 3 PB set-up and the value was found to be approximately 192 MPa. The material properties of the 0° layer in the skin and web were taken from [22] and given in Table 2. Note that the subscript 1 refers the longitudinal direction.

The parameters used in the traction separation law defined at the cohesive surface between the skin and filler were taken from [11] in which the mix mode cohesive properties were provided for a polyetheretherketone (PEEK) reinforced with AS4. Similar values were also used in the present study and corresponding values are given in Table 3. The values for the penalty stiffness (K_{nn}, K_{ss} and K_{tt} in Eq. 1) at the cohesive surface were taken as 10^6 N/mm^3 [11] in order not to affect the overall stiffness of the structure. Since the fracture in the filler material was observed as brittle in the experiments, a lower values were assumed for the critical energy release rates used in Eq. 10 in the VCCT. The corresponding values are given in Table 4.

As aforementioned, a thermal load was imposed by applying a temperature gradient (ΔT) to the butt jointed TPC. Since the PEKK is a semi-crystalline thermoplastic, there is hardly residual stresses built up until the stress free temperature which is the crystallization peak temperature (T_c) [15-18]. The crystalline phases have the load bearing capability below T_c and residual stresses are built up during cooling due to the mismatch in the thermal shrinkage behavior between the matrix and the fiber reinforcement. Therefore, the temperature drop from T_c to room temperature was considered as thermal load in this work. According to the manufacturer's data sheet for PEKK [23], the melting point is 337°C, glass transition temperature is 159°C and crystallization temperature (T_c) is 279°C. Hence, ΔT was assumed to be 260°C.

E_1 [GPa]	$E_2 = E_3$ [GPa]	G_{12} [GPa]	G_{23} [GPa]	α_1 [με/°C]	$\alpha_2 = \alpha_3$ [με/°C]
16.2	6.1	2.1	2	9	43

Table 1: The measured material properties of an aligned short carbon (AS4) reinforced PEKK.

E_1 [GPa]	$E_2 = E_3$ [GPa]	G_{12} [GPa]	G_{23} [GPa]	α_1 [με/°C]	$\alpha_2 = \alpha_2$ [με/°C]
134	9.65	5.3	3.32	3	44

Table 2: Material properties of a unidirectional AS4/PEKK layer [22].

G_{Ic} [kJ/m^2]	G_{IIc} [kJ/m^2]	G_{IIIc} [kJ/m^2]	η	t_n^o [MPa]	t_s^o [MPa]	t_t^o [MPa]
1	1.5	1.5	2.284	80	100	100

Table 3: Parameters used in the traction separation law for the cohesive surface.

G_I^c [kJ/m^2]	G_{II}^c [kJ/m^2]	G_{III}^c [kJ/m^2]
0.5	1	1

Table 4: Parameters used in the VCCT for the short fiber reinforced filler material.

4 RESULTS AND DISCUSSIONS

The residual stresses and shape distortions were predicted in the first step of the quasi static analysis. The residual distortions in the *y*-direction (U2) are shown in Fig. 5. It is seen that there is a residual warpage pattern found in the part. The internal stress level was calculated approximately as 70 MPa (maximum principle stress) for the filler. The residual stresses directly affect the crack initiation in the filler since the critical principal stress (S_c) was used for the crack initiation in the filler as mentioned in Section 3.

Subsequent to the thermal stress analysis, a displacement (d = 2.7 mm) acting on the negative *y*-direction was applied from the reference point (RP) of the loading pin which was modelled as a rigid surface (see Fig. 2). The reaction force as well as the displacement was retrieved at the RP. The predicted and measured force-displacement curves are depicted in Fig. 6. It is seen that there are three measured curves from experiments for three different skin thickness (h) values. In the numerical model, the mean thickness of these three specimens was used which was 2.32 mm. It is seen from 6 that the force dropped rapidly due to the fracture in the filler together with subsequent delamination at the skin-filler interface. The change in force was found to be approximately 150 N. The values for the force at fracture and displacement at fracture are given in Table 5. It should be noted that quite small time steps (~1e-8 s) were used in the quasi static analysis during the crack growth in the filler and delamination at the interface. Therefore, the analysis was stopped when the maximum drop in force was obtained which can be seen in Fig. 6. In order to obtain the similar magnitude of force at fracture as well as displacement at fracture as compared with the experiments, S_c was calibrated in the model to 185 MPa. If S_c is increased, then a much higher force and displacement at fracture would be obtained with the linear stiffness shown in Fig. 6. The calibrated S_c value (185 MPa) was found to be quite close to the transverse strength of the filler (192 MPa) measured under separate 3 PB tests for dog-bone specimens. It is also worth to mention that without taking the residual stresses into account, the crack initiated at S_c = 115 MPa while having the crack initiation in the filler at the similar force and displacement values provided in Table 5.

Fig. 7 shows the fracture behavior of the specimen taken by the high speed camera. According to the frames recorded by the camera, the crack first initiated in the filler then grew towards skin-filler interface in less than 33 μs. The unstable crack growth noticed on the force-displacement graph is supported by the high speed camera pictures, which shows that the butt joint is separated from the main laminate within 1 to 2 ms. The predicted crack growth in the filler and delamination at the sin-filler interface are shown in Fig. 8. It is seen that once the crack reaches the interface, the delamination starts immediately. The location of the crack growth and the delamination length were found to agree well with the experimental observations. In Fig. 8, the maximum principal stress distribution is also

shown. It is seen that peak stresses take place at the interface during delamination due to the presence of cohesive stresses. Before the fracture, the stress level was calculated approximately as 1070 MPa in the 0° layer of the skin which is in contact with the filler. The peak stress increased to a value of approximately 1500 MPa during the separation of filler from the skin. After delamination the stress level decreased to around 1225 MPa.

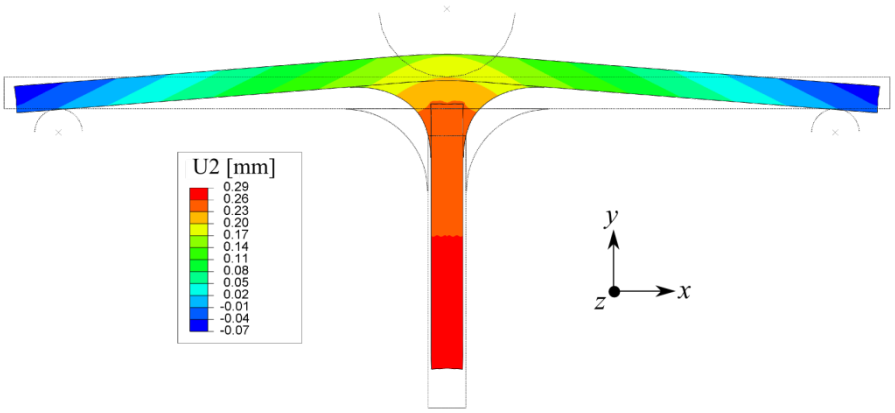

Figure 5: The residual deformations (U2) in the *y*-direction after applying a temperature gradient ΔT = -260°C. The undeformed geometry is shown with a wireframe.

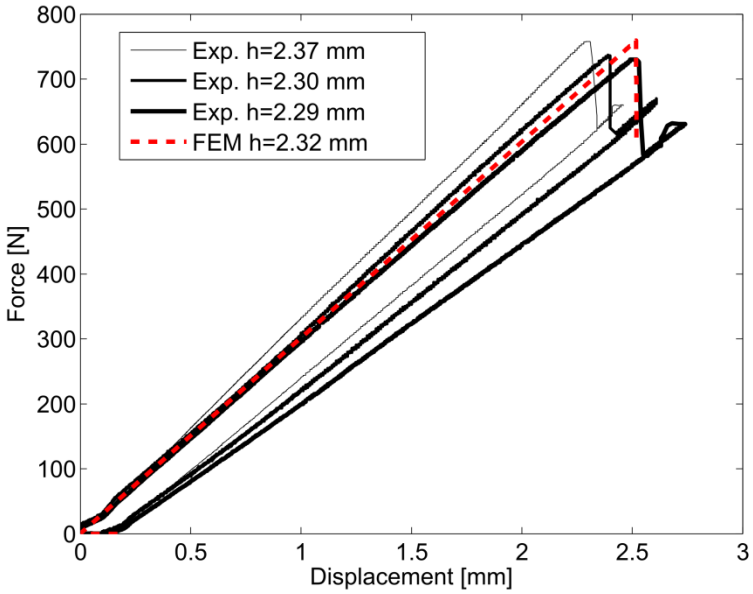

Figure 6: Force-displacement response under 3 PB conditions.

	Force at fracture [N]	**Displacement at fracture [mm]**
Exp. h = 2.29 mm	730	2.52
Exp. h = 2.30 mm	736	2.40
Exp. h = 2.37 mm	758	2.31
FEM h = 2.32 mm	759	2.52

Table 5: The force and displacement values at fracture.

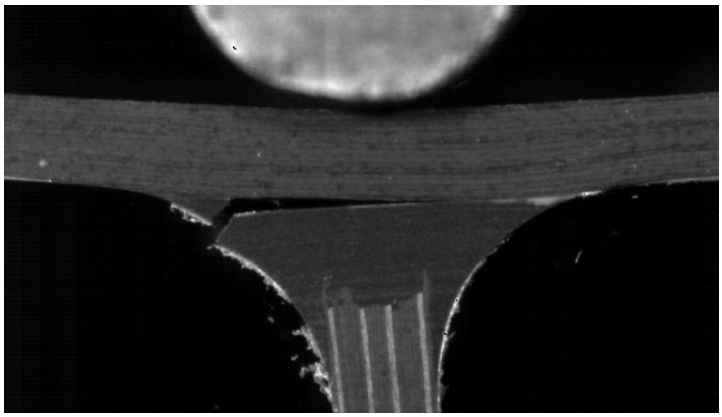

Figure 7: High speed camera shot at the end of the fracture.

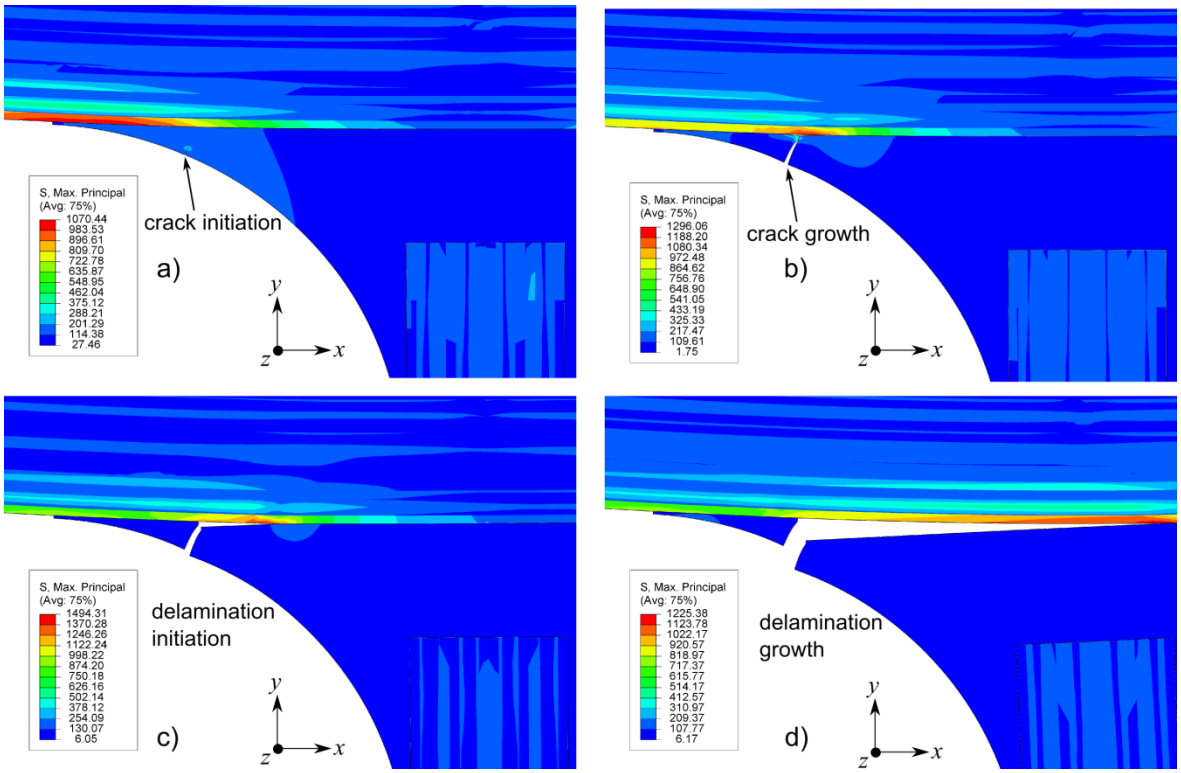

Figure 8: The predicted fracture behavior in the filler and at the skin-filler interface with maximum principal stress distribution [MPa]. a) crack initiation in the filler, b) crack growth in the filler, c) beginning of the delamination at the skin-filler interface and d) propagation of the delamination at the skin-filler interface.

5 CONCLUSIONS

The mechanical response of a hybrid thermoplastic structure under bending conditions was analyzed in this work. The tests were carried out using a 3PB set-up. The force-displacement response was recorded and the fracture behavior was captured using a high speed camera. The laminated skin and the web were manufactured using an autoclave tooling and the material was AS4/PEKK with a layup configuration $[0/45/-45/90/45/0/-45/90]_s$. Short fiber reinforced filler or butt joint material made of AS4/PEKK (20% filled) was injected molded to join the skin and the web.

A quasi-static analysis was carried out using a numerical model developed in ABAQUS. The crack initiation and growth in the filler were modelled using the VCCT. The subsequent delamination at the

skin-filler interface was predicted using the traction separation law with cohesive surface. In the model, the residual thermal stresses were also included by applying a temperature gradient from the crystallization temperature to room temperature. The critical strain energy release rate for the filler was taken smaller than the fracture energy of the cohesive surface at the skin-filler interface since a brittle crack growth was observed during the experiments. The predicted force-displacement response was found to be agree well with the experimental measurements by setting the critical principal stress (S_c) value to 185 MPa for the filler. Without taking the residual stresses into account, S_c was found to be 115 MPa while having the same force and displacement at fracture as compared with the experiments.

REFERENCES

[1] S.P. Haanappel and R. Akkerman, Shear characterisation of uni-directional fibre reinforced thermoplastic melts by means of torsion, *Composites Part A: Applied science and manufacturing*, **56**, 2014, pp. 8-26.

[2] S.P. Haanappel, R.H.W. ten Thije, U. Sachs, A.D. Rietman and R. Akkerman, Formability analyses of uni-directional and textile reinforced thermoplastics, *Composites Part A: Applied science and manufacturing*, **56**, 2014, pp. 80-92.

[3] W.J.B. Grouve, G. Vanden Poel, L. Warnet and R. Akkerman, On crystallisation and fracture toughness of poly(phenylene sulphide) under tape placement conditions, *Plastics rubber and composites*, **42 (7)**, 2013, pp. 282- 288.

[4] W.J.B. Grouve, L. Warnet and R. Akkerman, Critical assessment of the mandrel peel test for fiber reinforced thermoplastic laminates, *Engineering fracture mechanics*, **101**, 2013, pp. 96-108.

[5] G.B. McGuinness and C.M. ÓBrádaigh, Characterisation of thermoplastic composite melts in rhombus-shear: the picture-frame experiment, *Composites Part A: Applied Science and Manufacturing*, **29**, 1998, pp. 115-132.

[6] W.J.B. Grouve, L. Warnet, B. Rietman, H.A. Visser and R. Akkerman, Optimization of the tape placement process parameters for carbon–PPS composites, *Composites Part A: Applied science and manufacturing*, **50**, 2013, pp. 44-53.

[7] S.C. Mantell and G.S. Springer, Manufacturing process models for thermoplastic composites, *Journal of Composite Materials*, **26**, 1992, pp. 2348-2377.

[8] M. Hou, K. Friedrich and R. Scherer, Optimization of stamp forming of thermoplastic composite bends, *Composite Structures*, **27**, 1994, pp. 157-167.

[9] A.S. Tam and T.G. Gutowski, Ply-slip during the forming of thermoplastic composite parts, *Journal of Composite Materials*, **23**, 1989, pp. 587-605.

[10] J. Karger-Kocsis and K. Friedrich, Effect of temperature and strain rate on fracture toughness of PEEK and its short glass fiber composites, *Polymer*, **27**, 1986, pp. 1753–1760.

[11] P.P. Camanho, C.G. Davila and M.F. de Maura, Numerical simulation of mixed mode progressive delamination in composite materials, *Journal of Composite* Materials, **37**, 2003, pp. 1415-1438.

[12] P.P. Camanho, C.G. Dávila and S.T. Pinho, Fracture analysis of composite co-cured structural joints using decohesion elements, *Fatigue and Fracture of Engineering Materials and Structures*, **27**, 2004, pp. 745-757.

[13] P.P. Camanho, and C.G. Dávila, *Mixed-mode decohesion elements for the simulation of delamination in composite materials*, NASA-TM-2002-211737, 2002.

[14] ABAQUS 6.12 Reference Guide. Dassault systems; 2012.

[15] P.P. Parlevliet, H.E.N. Bersee and A. Beukers, Residual stresses in thermoplastic composites - A study of the literature - Part I: Formation of residual stresses, *Composites Part A: Applied Science and Manufacturing*, **37**, 2006, pp. 1847-1857.

[16] P.P. Parlevliet, H.E.N. Bersee and A. Beukers, Residual stresses in thermoplastic composites - A study of the literature - Part II: Experimental techniques, *Composites Part A: Applied Science and Manufacturing*, **38**, 2007, pp. 651-665.

[17] P.P. Parlevliet, H.E.N. Bersee and A. Beukers, Residual stresses in thermoplastic composites - A study of the literature - Part III: Effect of thermal residual stresses, *Composites Part A: Applied Science and Manufacturing*, **38**, 2007, pp. 1581-1596.

[18] M.L. Benzeggagh and M. Kenane, Measurement of mixed-mode delamination fracture toughness of unidirectional glass/epoxy composites with mixed-mode bending apparatus, *Composites Science and Technology*, **56**, 1996, pp. 439-449.

[19] E.F. Rybicki and M.F. Kanninen, A finite element calculation of stress intensity factors by a modified crack closure integral, *Engineering Fracture Mechanics*, **9**, 1977, pp. 931-938.

[20] E.F. Rybicki, D.W. Schmueser and J. Fox, An energy release rate approach for stable crack growth in the free-edge delamination problem, *Journal of Composite Materials*, **11**, 1977, pp. 470-487.

[21] R. Krueger, Virtual crack closure technique: History, approach, and applications, *Applied Mechanics Reviews*, **57**, 2004, pp. 109-143.

[22] K. Ilin, L.L.Warnet, B. Rietman, R. Akkerman and R.H.W. ten Thije, Failure modeling of thermoplastic butt-joint stiffened panels by quasi-static loading, *Proceedings of the SIMULIA Community Conference*, 2012.

[23] Technical data sheet: PEKK Thermoplastic polymer, CYTEC, 2012.